Electronic Supplementary Information

Cu doping in CeO_2 to form multiple oxygen vacancies for dramatically enhanced ambient N_2 reduction performance

Shengbo Zhang,[†ab] Cuijiao Zhao,[†ab] Yanyan Liu,[ab] Wenyi Li,[ab] Jialu Wang,[ab] Guozhong Wang,[a] Yunxia Zhang,[a] Haimin Zhang,*[a] and Huijun Zhao[ac]

[a.] *Key Laboratory of Materials Physics, Centre for Environmental and Energy Nanomaterials, Anhui Key Laboratory of Nanomaterials and Nanotechnology, CAS Center for Excellence in Nanoscience, Institute of Solid State Physics, Chinese Academy of Sciences, Hefei 230031, China. E-mail:* zhanghm@issp.ac.cn

[b.] *University of Science and Technology of China, Hefei 230026, China.*

[c.] *Centre for Clean Environment and Energy, Griffith University, Gold Coast Campus, QLD 4222, Australia.*

Experimental Section

Preparation of CeO_2 and Cu-CeO_2-x (x= 2.2, 3.9, 5.7, 7.7, 8.2). All of the chemical regents were analytical grade (AR) and were used without further purification. A hydrothermal method was used to synthesize CeO_2 nanorods.[1] Typically, 0.88 g $Ce(NO_3)_3$ $6H_2O$ (Sinopharm Chemical Reagent Co., China) was dissolved in 20 mL of deionized (DI) water with stirring to obtain a homogeneous solution. Then 8.44 g NaOH (Sinopharm Chemical Reagent Co., China) was dissolved in 15 mL of deionized water. The prepared NaOH solution was added dropwise to the above $Ce(NO_3)_3$ solution with gentle stirring at room temperature. The mixed solution was adequately stirred for additional 30 min at room temperature and then transferred into Teflon-lined stainless steel autoclave (50 mL) for hydrothermal reaction at 100 ℃ for 24 h. After the reaction, the autoclave was cooled down to room temperature, the obtained white precipitate was collected and washed with deionized water and ethanol for several times in order to remove the residual reactants, Finally, the precipitate was dried in oven at 60 ℃ for 16 h. The obtained pale yellow powder was subsequently calcined in a tube furnace under Ar atmosphere at 500 ℃ for 4 h to obtain pure CeO_2 sample. The CeO_2 was then used as precursor to fabricate Cu-CeO_2-x sample (x represents the mass content (wt.%) of the doped Cu, determined by inductively

coupled plasma optical emission spectroscopy (ICP-OES)). For instance, to fabricate Cu-CeO_2-3.9 sample, 400 mg CeO_2 was dispersed into 10 mL of deionized water under ultrasonication, and 63.6 mg $Cu(NO_3)_2$ $3H_2O$ (99% purity, Sinopharm Chemical Reagent Co., Ltd., China) was added to the above solution. After stirring for 10 min, 5 mL of aqueous solution containing 250 mg of Na_2CO_3 (Sinopharm Chemical Reagent Co., Ltd) was added to the above mixture. The obtained suspension was then stirred at room temperature for 2 h, then filtered and thoroughly washed with hot deionized water, followed by drying at 60 ^oC in an oven for overnight and finally thermally treating in H_2 and Ar mixture (H_2 Vol. ratio of 5%) at 250 ^oC for 1 h (temperature ramping rate of 5 ^oC min^{-1}). The Cu doped CeO_2 sample with other Cu doping content was also fabricated using similar synthesis procedure.

Characterization. The crystalline structures of samples were identified by X-ray diffraction analysis (XRD, Philips X'pert PRO) using Nifiltered monochromatic CuKa radiation (λKα1 = 1.5418 Å) at 40 kV and 40 mA. Transmission electron microscope (TEM) images of samples were obtained using JEMARM 200F operating at an accelerating voltage of 200 kV. High-resolution transmission electron microscope (HRTEM), scanning TEM images (STEM) and elemental mapping images of samples were obtained on a JEOL-2010 transmission electron microscope. Furthermore, the spherical aberration corrected (Cs-corrected) high angle annular dark field scanning transmission electron microscopy (HAADF-STEM) and the energy-dispersive X-ray (EDX) mapping experiments were performed using FEI Titan G2 microscope equipped with a Super-X detector at 300 kV. X-ray photoelectron spectroscopy (XPS) analysis was performed on an ESCALAB 250 X-ray photoelectron spectrometer (Thermo, America) equipped with Al Kα1, 2 monochromatized radiations at 1486.6 eV Xray source. The Cu doping content in CeO_2 nanorods was determined using inductively coupled plasma atomic emission spectrometer (ICP-AES, ICP-6300, Thermo Fisher Scientific). Nitrogen adsorption-desorption isotherms were measured using an automated gas sorption analyzer (Autosorb-iQ-Cx). The Cu $L_{3,2}$-edge absorptoion near-edge spectra (XANES) of samples were measured at BL12B-a beamline of NSRL in the total electron yield

(TEY) mode by collecting the sample drain current under a vacuum better than 5×10^{-8} Pa. The beam from the bending magnet was monochromatized utilizing a varied linespacing plane grating and refocused by a toroidal mirror. The energy range is 100-1000 eV with an energy resolution of ca. 0.1 eV. The ^{15}N isotopic labeling experiments were conducted using $^{15}N_2$ as the feeding gas (99% enrichment of ^{15}N in $^{15}N_2$, Supplied by Hefei Ninte Gas Management Co., LTD). Prior to use for NRR measurements, $^{15}N_2$ feeding gas was purged through a 1.0 mM H_2SO_4 solution and distilled water to eliminate the potential NO_x and NH_3 contaminants.[2] The ^1H NMR (nuclear magnetic resonance) spectra were obtained using superconducting Fourier transform nuclear magnetic resonance spectrometer (Bruker Avance−400). $(^{15}NH_4)_2SO_4$ as reference samples was dissolved in 0.1 M Na_2SO_4 solution (D_2O/H_2O mixed solution, $V_{D2O}:V_{H2O}$ =1:4) for ^1H NMR measurements, and the electrolyte obtained from $^{15}N_2$-saturated 0.1 M Na_2SO_4 solution with the reaction time of 2 h and concentration time of 12 h at 80 ^oC (D_2O/electrolyte mixed solution, $V_{D2O}:V_{electrolyte}$ =1:4) for ^1H NMR measurements.

Electrochemical measurements. All electrochemical measurements were performed on a CHI 660E electrochemical workstation (CH Instrumental Corporation, Shanghai, China) using a two-compartment cell, which was separated by Nafion 211 membrane. Different catalyst inks were prepared by dispersing 4.0 mg sample into 200 μL of ethanol and 10 μL of Nafion (5 wt.%) under ultrasonic, and were then dropped on carbon cloth with 1×1 cm^2 used as the working electrode. A Ag/AgCl electrode was used as the reference electrode and a Pt wire was used as the counter electrode. The polarization curves were measured with a scan rate of 5.0 mV s^{-1} at room temperature and all polarization curves were obtained at the steady-state ones after several cycles. For N_2 reduction reaction (NRR) experiments, the potentiostatic test was conducted for 2 h in N_2-saturated 0.1 M Na_2SO_4 solution (30 mL, pH=6.3) by continuously supplying N_2 into the electrolyte under ambient conditions. Prior to NRR measurements, N_2 feeding gas was first purged through a 1.0 mM H_2SO_4 solution and distilled water to eliminate the potential NO_x and NH_3 contaminants. In this work, all

measured potentials (*vs.* Ag/AgCl) were transformed into the potentials *vs.* reversible hydrogen electrode (RHE) based on the following equation:

$$E_{\mathrm{RHE}} = E_{\mathrm{Ag/AgCl}} + 0.059\mathrm{pH} + E^{\circ}_{\mathrm{Ag/AgCl}}$$

Determination of ammonia. Concentration of the produced ammonia was spectrophotometrically detected by the indophenol blue method. In detail，5 mL of sample was taken, and then diluted with 5 mL of deionized water. Subsequently, 100 μL of oxidizing solution (sodium hypochlorite (ρCl=4~4.9) and 0.75 M sodium hydroxide), 500 μL of colouring solution (0.4 M sodium salicylate and 0.32 M sodium hydroxide) and 100 μL of catalyst solution (0.1g $Na_2[Fe(CN)_5NO]$ $2H_2O$ diluted to 10 mL with deionized water) were added respectively to the measured sample solution. After the placement of 1 h in room temperature, the absorbance measurements were performed at wavelength of 697.5 nm. The obtained calibration curve (Fig. S7) was used to calculate the ammonia concentration.

Determination of hydrazine. The hydrazine present in the electrolyte was estimated by the method of Watt and Chrisp. A mixture of para-(dimethylamino) benzaldehyde (5.99 g), HCI (concentrated, 30 mL) and ethanol (300 mL) was used as a color reagent. In detail，5 mL of sample with 0.1 M HCl solution was taken, and then 5 mL of the prepared color reagent was added to the above sample solution. Subsequently, the absorbance measurements were performed after the placement of 20 min at wavelength of 455 nm. The obtained calibration curve (Fig. S8) was used to calculate the $N_2H_4 \cdot H_2O$ concentration.

Calculations of NH_3 production rate and Faradaic efficiency.

The equation of NH_3 production rate:

$$R(\mathrm{NH_3})(\mathrm{mol\ cm^{-2}\ s^{-1}}) = \frac{\chi(\mathrm{ppm}) \times 10^{-3}(\mathrm{g\ mg^{-1}}) \times V(\mathrm{L})}{\mathrm{Mr}_{\mathrm{NH_4^+}-N}(\mathrm{g\ mol^{-1}}) \times t(\mathrm{s}) \times S(\mathrm{cm^{-2}})}$$

where $R(NH_3)$ is the ammonia production rate in mol cm^{-2} s^{-1}; χ (ppm) is the produced ammonia concentration; V (L) is the electrolyte solution volume; Mr_{NH4^+-N}=14 (g mol^{-1}); t (s) is the reaction time; S is the geometric area of the cathodic electrode in cm^{-2}, and in this work two sides of the carbon cloth electrode are electrocatalytically active for the NRR, thus the NH_3 production rate is calculated by dividing the total

geometric area of two sides of the carbon cloth electrode.

The equation of Faradaic efficiency:

$$FE(\mathrm{NH_3})(\%) = \frac{3 \times n(\mathrm{NH_3})(\mathrm{mol}) \times F}{Q} \times 100\%$$

where F is the Faradaic constant (96485.34); Q is the total charge during the NRR.

Supplementary Tables and Figures

Table S1 The doped Cu content in different samples determined by ICP-OES.

Sample	Cu (mg)	Cu (μmol)	Mass Content (wt.%)
Cu-CeO_2-2.2	0.11	1.71	2.2
Cu-CeO_2-3.9	0.19	3.01	3.9
Cu-CeO_2-5.7	0.29	4.48	5.7
Cu-CeO_2-7.7	0.38	5.98	7.7
Cu-CeO_2-8.2	0.41	6.35	8.2

Table S2 The comparable results of our work and other recently reported transition metal oxides NRR electrocatalysts.

References	Catalyst	System /Conditions	NH_3 Production Rate	Faradaic Efficiency (%)	Detection method
3	Fe_2O_3-CNTs	diluted $KHCO_3$ aqueous solution	4.7×10^{-10} mol cm^{-2} s^{-1} （-1.0V *vs.* Ag/AgCl）	0.15	Indophenol method
4	Fe_2O_3 Nanorod	0.1 M Na_2SO_4	15.9 μg h^{-1} mg_{cat}^{-1} (-0.8 V *vs.* RHE)	0.94	Indophenol method
5	Fe/Fe Oxide	0.1 M PBS	0.19 μg cm^{-2} h^{-1} (-0.3 V *vs.* RHE)	8.29	Indophenol method
6	Fe_3O_4 nanorod	0.1 M Na_2SO_4	5.6×10^{-11} mol cm^{-2} s^{-1} (-0.4V *vs.* RHE)	2.6	Indophenol method
7	Mn_3O_4 nanocube	0.1 M PBS	11.6 μg h^{-1} mg^{-1}_{cat} (0.8V *vs.* RHE)	3.0	Indophenol method
8	Cubic sub-micron SnO_2 particle	0.1 M Na_2SO_4	1.47×10^{-10} mol s^{-1} cm^{-1} (-0.8 V *vs.* RHE)	2.17	Indophenol method
9	MoO_3 nanosheet	0.1 M HCl	4.8×10^{-10} mol s^{-1} cm^{-1} (-0.1 V *vs.* RHE)	1.9	Indophenol method
10	NbO_2	0.05 M H_2SO_4	2.3×10^{-10} mol s^{-1} cm^{-1} (-0.6 V *vs.* RHE)	32.0	Indophenol method
11	Y_2O_3 nanosheet	0.1 M Na_2SO_4	1.06×10^{-10} mol s^{-1} cm^{-1} (-0.9 V *vs.* RHE)	2.53	Indophenol method
12	$BiVO_4$	0.2 M Na_2SO_4	1.41×10^{-10} mol s^{-1} cm^{-1} (-0.5 V vs. RHE)	10.04	Indophenol method
13	MnO	0.1 M Na_2SO_4	1.11×10^{-10} mol s^{-1} cm^{-1} (-0.39 V vs. RHE)	8.02	Indophenol method
14	TiO_2 nanosheets	0.1 M Na_2SO_4	9.16×10^{-11} mol s^{-1} cm^{-1} (-0.8 V vs. RHE)	2.50	Indophenol method
15	Cr_2O_3 microspheres	0.1 M Na_2SO_4	2.4×10^{-9} mol s^{-1} cm^{-2} (-0.9 V vs. NHE)	6.78	Indophenol method
16	VO_2	0.1 M Na_2SO_4	14.85 μg h^{-1} mg_{cat}^{-1} (-0.9 V vs. NHE)	3.97	Indophenol method
17	TiO_2-rGO	0.1 M Na_2SO_4	15.13 μg h^{-1} mg_{cat}^{-1} (-0.9 V vs. NHE)	3.3	Indophenol method

18	C-TiO_2	0.1 M Na_2SO_4	16.22 μg h^{-1} mg_{cat}^{-1} (-0.7 V vs. NHE)	1.84	Indophenol method
This work	Cu-doped CeO_2 nanorods	0.1 M Na_2SO_4	5.3×10^{-10} mol s^{-1} cm^{-1} or 13.3 μg h^{-1} mg_{cat}^{-1} (-0.45 V *vs.* RHE)	19.1	Indophenol method

Table S3 High-resolution Ce 3d and Cu 2p XPS results. The listed-out figures are the binding energies (BE) and the area of each peak. The ratio of Ce^{3+}/Ce^{4+} ($Cu^{0,+1}/Cu^{2+}$) was calculated to illustrate the content of oxygen vacancy around Ce^{3+} sites on catalyst surface.

	Binding energy (eV)	**CeO_2**	**Cu-CeO_2-2.2**	**Cu-CeO_2-3.9**	**Cu-CeO_2-8.2**
μ‴	916.7	59222.6	44263.6	35456.5	37335.7
μ″	907.3	52442.3	48761.2	38074.5	34390
μ′	903.7	41601.9	28901	24844.7	18337.3
μ	900.8	68581	30243.8	30568.8	32203.5
μ_o	899.1	46888	23404.2	22618.5	26667.7
ν‴	898.3	63378.7	50908.1	47211.9	45212.8
ν″	888.6	51936.6	34228.6	44177.9	26299.5
ν′	885.3	51954.2	35553.3	33305.7	15598.7
ν	882.7	69926.5	59881.6	46213.3	32387.9
ν_o	880.7	38427.8	18925.9	14571.4	10885.1
	Ce^{4+}	365487.7	268286.9	241702.9	207829.4
	Ce^{3+}	178871.9	106782.4	95340.3	71488.8
	Ce^{3+}/Ce^{4+}	0.489	0.398	0.394	0.345
$Cu^{0,+1}$	932.8		1912.846	4586.9	13504.13
Cu^{2+}	935.2		5322.846	6856.9	17704.13
	$Cu^{0,+1}/Cu^{2+}$		0.359	0.669	0.763

Peaks μ′, μ_o, ν′ and ν_o belong to Ce^{3+}.

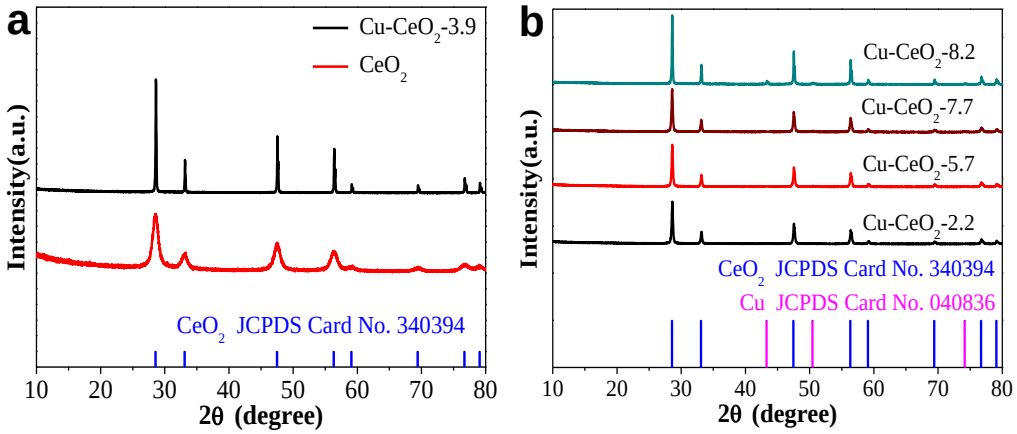

Fig. S1 XRD patterns of (a) pure CeO_2 and Cu-CeO_2-3.9 samples, and (b) Cu-CeO_2-2.2, Cu-CeO_2-5.7, Cu-CeO_2-7.7 and Cu-CeO_2-8.2 samples.

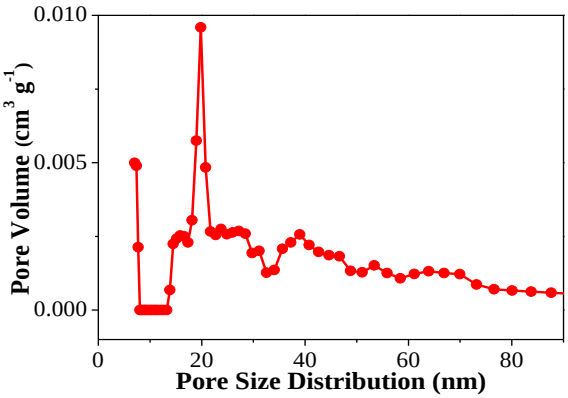

Fig. S2 The pore size distribution curve of Cu-CeO_2-3.9 sample.

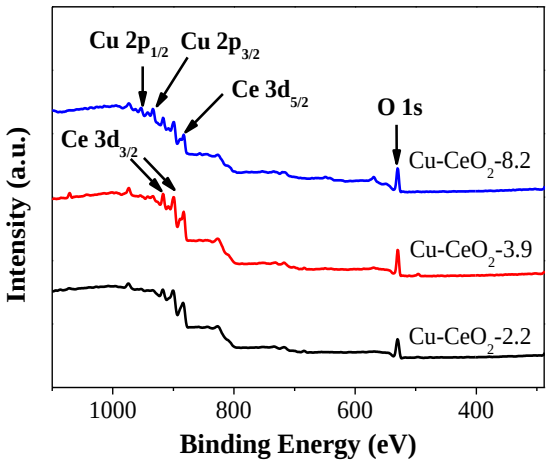

Fig. S3 The surface survey XPS spectra of Cu-CeO_2-2.2, Cu-CeO_2-3.9 and Cu-CeO_2-8.2 samples.

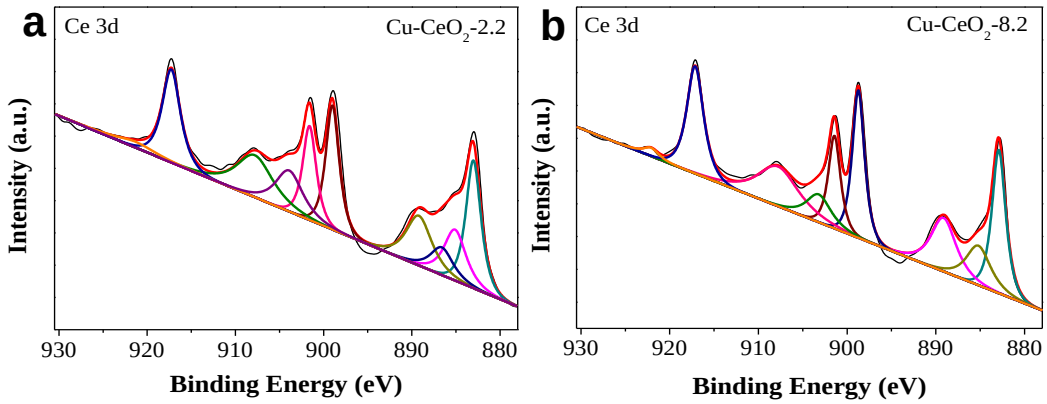

Fig. S4 Ce 3d XPS spectra of (a) Cu-CeO_2-2.2 and (b) Cu-CeO_2-8.2 samples.

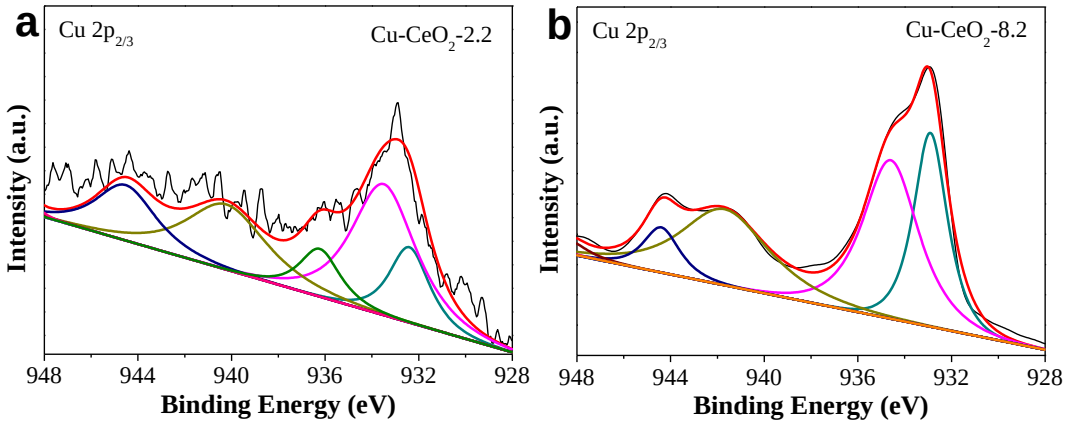

Fig. S5 Cu 2p XPS spectra of (a) Cu-CeO_2-2.2 and (b) Cu-CeO_2-8.2 samples.

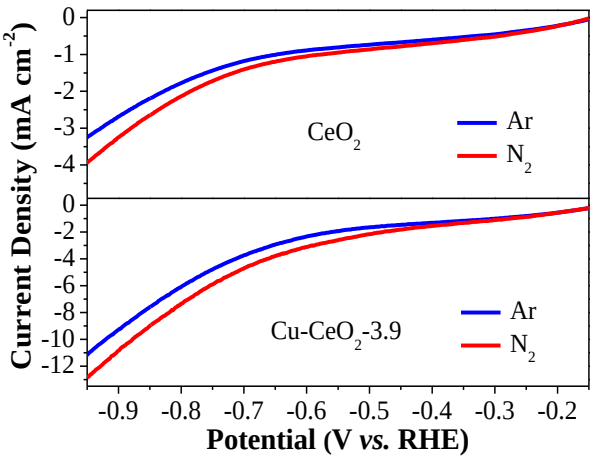

Fig. S6 Linear sweep voltammogram (LSV) curves of pure CeO_2 nanorods and Cu-CeO_2-3.9 nanorods catalysts in Ar- or N_2-saturated 0.1 M Na_2SO_4 solution (pH=6.3). The scan rate of 5.0 mV s^{-1}.

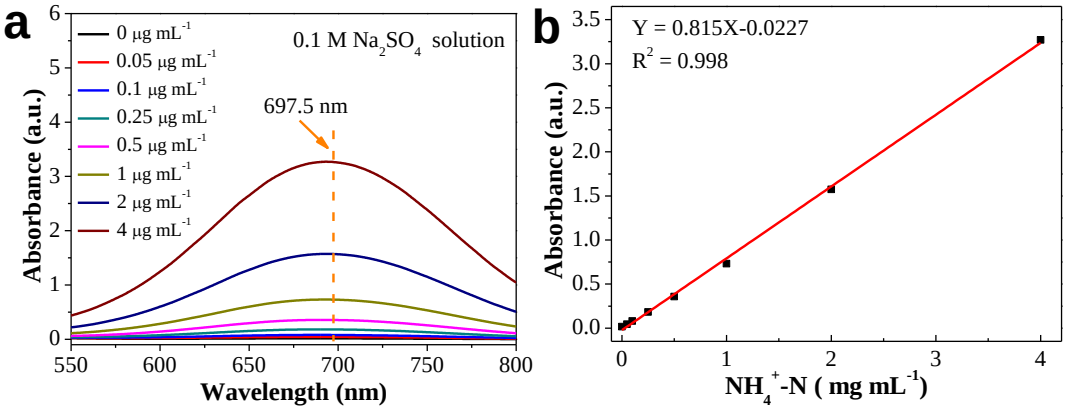

Fig. S7 (a) UV-Vis absorption spectra of various NH_4^+-N concentrations (0, 0.05, 0.1, 0.25, 0.5, 1, 2 and 4 μg mL^{-1}) after incubated for 1 h at room temperature. (b) The calibration curve used for calculation of NH_4^+-N concentration.

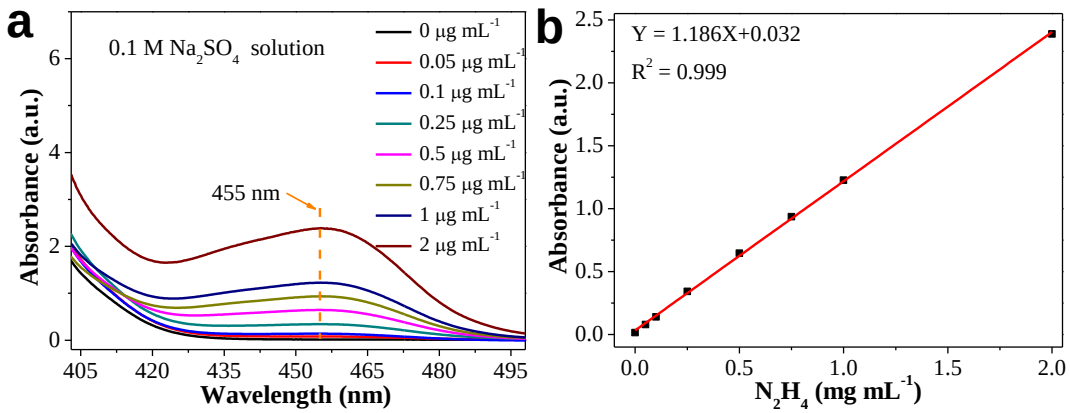

Fig. S8 (a) UV-Vis absorption spectra of various $N_2H_4 \cdot H_2O$ concentrations (0, 0.05, 0.1, 0.25, 0.5, 0.75, 1 and 2 μg mL^{-1}) after incubated for 20 min at room temperature. (b) The calibration curve used for calculation of $N_2H_4 \cdot H_2O$ concentrations.

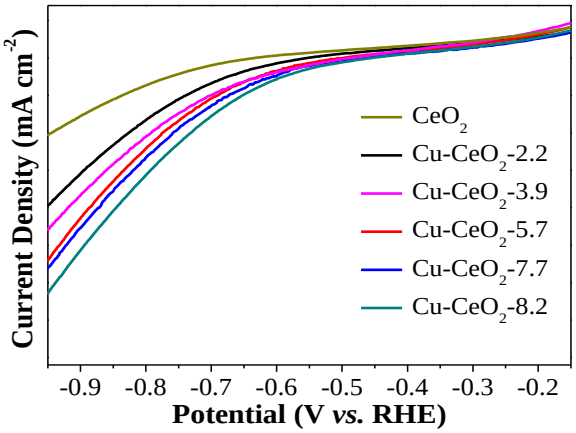

Fig. S9 Linear sweep voltammogram (LSV) curves of pure CeO_2 nanorods and Cu-doped CeO_2 nanorods catalysts with different Cu doping contents in Ar-saturated 0.1 M Na_2SO_4 solution (pH=6.3). The scan rate of 5.0 mV s^{-1}.

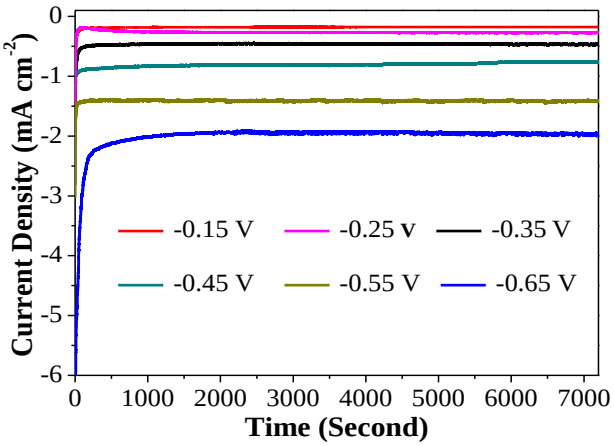

Fig. S10 Chrono-amperometry curves of Cu-CeO_2-3.9 catalyst obtained at different applied potentials in N_2-saturated 0.1 M Na_2SO_4 solution.

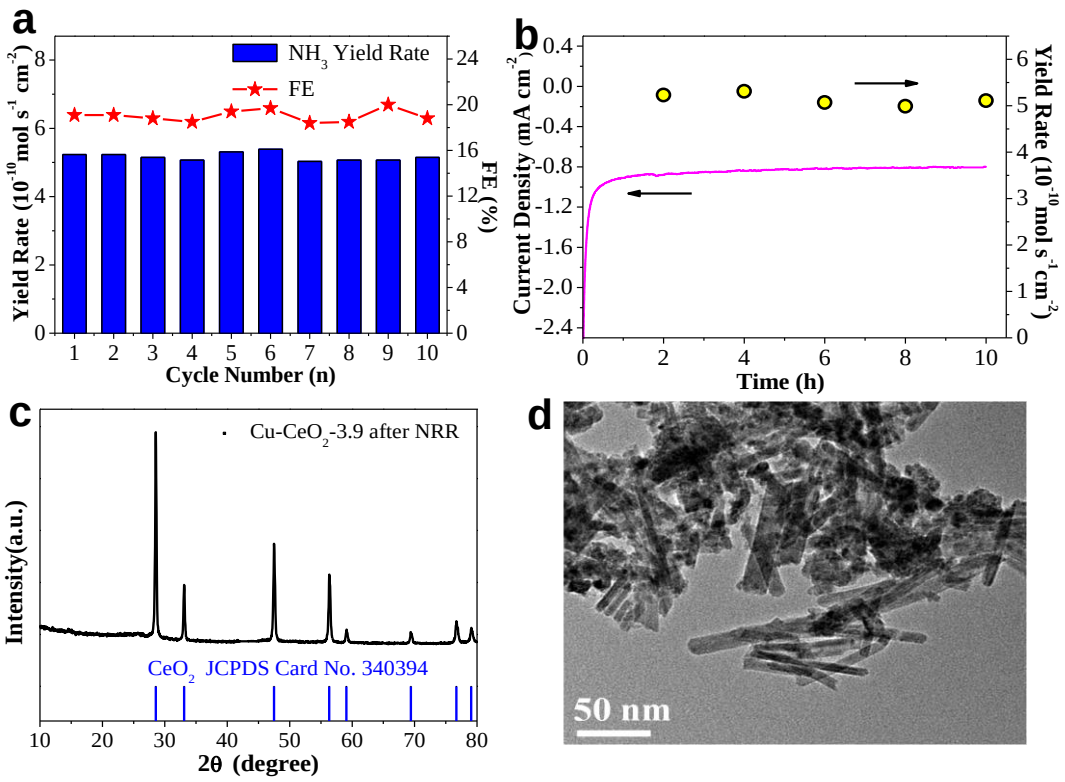

Fig. S11 (a) NH_3 yield rates and Faradaic efficiencies of the Cu-CeO_2-3.9 after consecutive recycling electrolysis in N_2-saturated 0.1 M Na_2SO_4 solution (pH=6.3) at -0.45 V *vs.* RHE for 2 h of each NRR experiment. (b) The durability test of Cu-CeO_2-3.9 obtained at -0.45 V (*vs.* RHE) for 10 h. (c) XRD patterns and (d) TEM image of the Cu-CeO_2-3.9 catalyst after durability test.

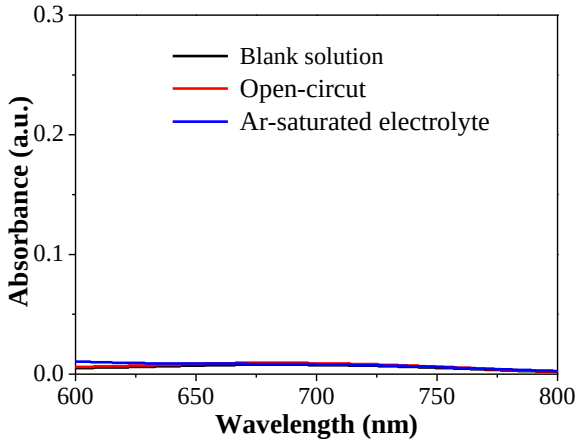

Fig. S12 UV-vis absorption spectra of the 0.1 M Na_2SO_4 electrolyte stained with indophenol indicator after charging at -0.45 V (*vs.* RHE) for 2 h under various conditions.

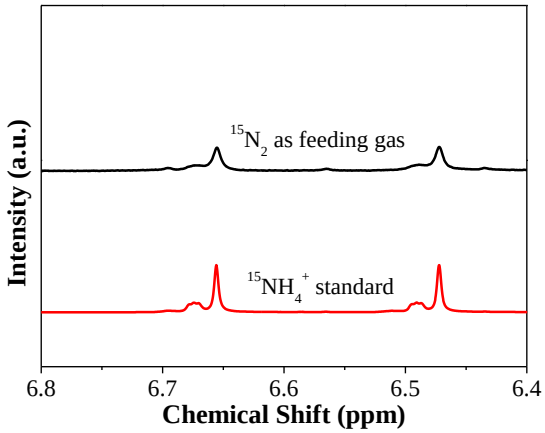

Fig. S13 The ^{1}H NMR spectra of the NRR sample using $^{15}N_2$ as the feeding gas and $^{15}NH_4^+$ standard.

As shown in Fig. S13, the ^{1}H NMR spectrum of the NRR sample using $^{15}N_2$ as the feeding gas obtained at -0.45 V (*vs.* RHE) for 2 h shows two resonance peaks in the range of 6.4–6.7 ppm. These two peaks match well with the reference substance ($^{15}NH_4^+$), further confirming that the determined NH_3 product in our work is indeed resulted from the Cu-CeO_2-3.9 catalyzed NRR process.

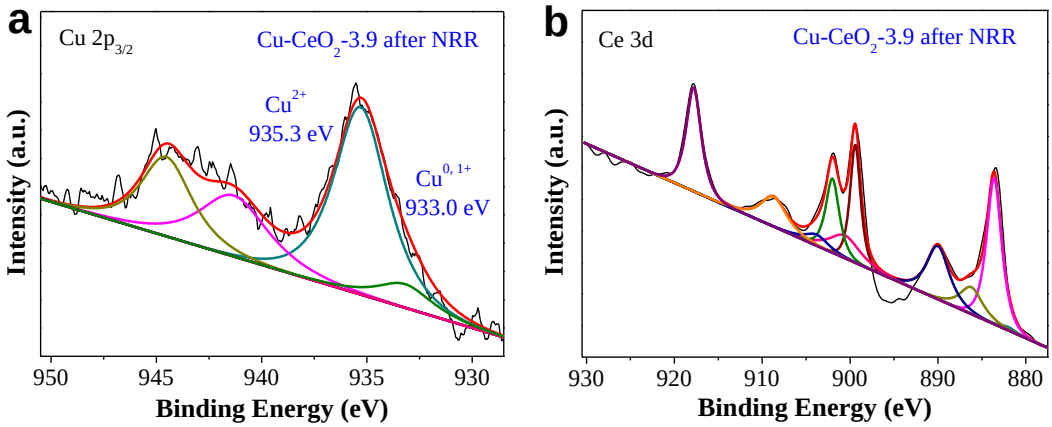

Fig. S14 (a) Cu 2p and (b) Ce 3d XPS spectra of the Cu-CeO_2-3.9 catalyst after NRR test.

References

1 Y. F. Wang, Z. Chen, P. Han, Y. H. Du, Z. X. Gu, X. Xu, and G. Zheng, *ACS Catal.*, 2018, **8**, 7113-7119.

2 F. Zhou, L. M. Azofra, M. Ali, M. Kar, A. N. Simonov, C. McDonnell-Worth, C. Sun, X. Zha ng, D. R. MacFarlane, *Energy Environ. Sci*., 2017, **10**, 2516.

3 S. Chen, S. Perathoner, C. Ampelli, C. Mebrahtu, D. Su and G. Centi, *Angew. Chem.*, *Int. Ed.*, 2017, **56**, 2699-2703.

4 X. Xiang, Z. Wang, X. Shi, M. K. Fan, and X. Sun, *ChemCatChem.*, 2018, **10**, 1-7.

5 L. Hu, A. Khaniya, J. Wang, G. Chen, W. E. Kaden, and X. F. Feng, *ACS Catal.*, 2018, **8**, 9312-9319.

6 Q. Liu, X. Zhang, B. Zhang, Y. Luo, G. Cui, F. Xie and X. Sun, *Nanoscale*, 2018, **10**, 14386-14389.

7 X. Wu, L. Xia, Y. Wang, W. Lu, Q. Liu, X. Shi, and X. Sun, *Small*, 2018, **14**, 1803111.

8 L. Zhang, X. Ren, Y. L. Luo, X. F. Shi, A. M. Asiri, T. Li and X. Sun, *Chem. Commun.*, 2018, **54**, 12966-12969.

9 J. Han, X. Ji, X. Ren, G. Cui, L. Li, F. Xie, H. Wang, B. Li and X. Sun, *J. Mater. Chem. A*, 2018, **6**, 12974-12977.

10 L. Huang, J. Wu, P. Han, A. M. Al-Enizi, T. M. Almutairi, L. Zhang, and G. Zheng, *Small Methods*, 2018, 1800386.

11 X. Li, L. Li, X. Ren, D. Wu, Y. Zhang, H. M. Ma, X. Sun, B. Du, Q. Wei, and B. Li, *Ind. Eng. Chem. Res.*, 2018, **57**, 16622–16627.

12 J. - X. Yao, D. Bao, Q. Zhang, M. - M. Shi, Y. Wang, R. Gao, J. - M. Yan, Q. Jiang, *Small Methods*, 2018, 1800333.

13 L. Zhang, X. Ji, X. Ren, Y. Luo, X. Shi, A. M. Asiri, B. Z. Zheng, and X. Sun, *Adv. Sci.*, 2019, **6**, 1801182.

14 R. Zhang, X. Ren, X. Shi, F. Xie, B. Zheng, X. Guo and X. Sun, *ACS Appl. Mater. Interfaces*, 2018, **10**, 28251-28255.

15 H. Du, X. Guo, R. Kong and F. Qu, *Chem. Commun.*, 2018, **54**, 12848-12851.

16 R. Zhang, H. Guo, L. Yang, Y. Wang, Z. Niu, H. Huang, H. Chen, L. Xia, T. Li, X. Shi, X. Sun, B. Li, and Q. Liu, *ChemElectroChem.*, 2018. 1801484.

17 X. Zhang, Q. Liu, X. Shi, A. M. Asiri, Y. Luo, X. Sun and T. Li, *J. Mater. Chem. A*, 2018, **6**, 17303-17306.

18 K. Jia, Y. Wang, Q. Pan, B. Zhong, Y. Luo, G. Cui, X. Guo and X. Sun, *Nanoscale Adv.*, 2019, doi: 10.1039/c8na00300a.